Three-dimensional optical metrology with extended depth-measuring range using a holographic axilens

Erez Hasman, MEMBER SPIE
Vladimir Kleiner
Technion-Israel Institute of Technology
Faculty of Mechanical Engineering
Optical Engineering Laboratory
Haifa 32000, Israel

Abstract. A method of 3-D optical metrology based on a triangulation system using holographic axilens to increase the depth-measuring range without any decrease in the axial or the lateral resolution is presented. The element is designed according to an analytic ray-tracing optimization approach and is recorded as a computer-generated hologram. A sixfold increase in the depth-measuring range is experimentally obtained while nearly diffraction limited light spots are completely maintained. © 2003 Society of Photo-Optical Instrumentation Engineers. [DOI: 10.1117/1.1524170]

Subject terms: metrology; holography; resolution; focus.

1 Introduction

The increasing demand for noncontact surface displacement and profile measurements has already led to the development of several electro-optical systems. These systems incorporate interferometry methods, speckle detection, Moiré deflectometry,[1] stereo vision, focus error detection,[2] time of flight, and structured light triangulation.[3,4] Noncontact electro-optical measuring systems are advantageous over those using mechanical sensing due to their relatively high speed and nondestructive capabilities.

The structured light triangulation method is the most widespread and is suitable for industrial applications in that it offers a simple and robust 3-D measurement. Structured light triangulation systems determine distance by projecting light from a source onto an object and imaging the resulting illumination pattern onto a detector. Knowing the position of the image on the detector, the lateral separation between the detector lens and the light source, and the projection angle of the source enables determination of the distance to the object. Sequential measurements at different coordinates on the object lead to a full 3-D image of the object surface.

The simplest structured light system projects a single point of light from the source onto an object. The point is then imaged on lateral-effect photodiodes or a linear array as the detector. This imaging is done point by point until the surface is scanned completely. This 3-D measurement procedure can be inexpensive and has a high resolution.

Unfortunately, the conventional light triangulation systems cannot simultaneously achieve a large depth-measuring range and high horizontal resolution. This is so because the conventional optical lenses that are incorporated in these systems cannot, at the same time, provide both long focal depth and high lateral resolution. Specifically, a high lateral resolution requires high numerical apertures, whereas a large depth of focus requires low numerical apertures. Thus, in general, there is a trade-off between range of depth and lateral resolution. Mathematically, the combination of Abbe's formula for lateral resolution ($1/\Delta x$), where Δx is the spot size, and Rayleigh's formula for the depth of focus δF yields

$$\delta F = \frac{k(\Delta x)^2}{\lambda}, \tag{1}$$

where λ is the wavelength of the light, and k is a constant number between 1 and 6, depending on the exact definitions of Δx and δF and on the wavefront apodization.

A common trade-off approach is to use a relatively large spot, the center of which can be determined, with much higher accuracy than the spot size, by complicated numerical techniques. Unfortunately, this approach is highly sensitive to local changes in the reflectivity or the shape of the object (e.g., short radius of curvatures cannot be adequately dealt with).

A novel single-point triangulation system has been developed based on an aspherical holographic optical element to achieve surface mapping with a high depth-measuring range and good vertical and horizontal resolution. We investigated special aspheric holographic elements that can have an arbitrarily long focal depth as well as a high lateral resolution. This element essentially combines the properties of the long focal depth of an axicon[5,6] and the high energy concentration of a conventional spherical lens, which has been called an axilens.[7] The design procedure of the axilens is based on an analytic ray-tracing approach.[8]

In this paper, we present a theoretical and experimental investigation of the 3-D optical profilometry, demonstrating a sixfold increase in the depth-measuring range while nearly diffraction limited light spots were completely maintained. Our experiments yield 3-D surface measurements with lateral and depth optical resolutions of <0.6 μm for a depth of focus of about 60 mm, resulting in $>10^5$ resolving depth steps.
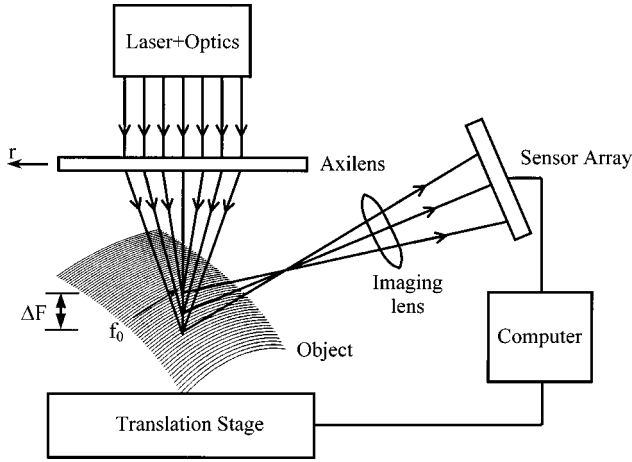
Fig. 1 Optical triangulation system with extended depth-measuring range based on a holographic axilens.

2 Design Procedure of the Profilometer Using the Axilens

The operation of our triangulation optical profilometry using a holographic axilens is described with reference to Fig. 1. A collimating lens system forms a plane wave from the laser source that is focused by the holographic axilens to an extended focal depth ΔF. An object with a maximum height difference smaller than the extended focal depth of the axilens, is placed in the region of the focused light. The object intersects the light, and the intersection point is then imaged with an off-axis configuration (at an angle θ from the illumination optical axis) to a 1-D or 2-D CCD camera. The data that are detected by the CCD camera are displayed on a monitor and processed by the computer to give the intersection point in virtually real time. After a single point is detected, a computer-controlled stepper motor shifts the object to get another point, and so on, until a complete 3-D profile of the object is obtained.

The design of the holographic axilens was optimized with an analytic ray-tracing approach.[8–10] To find the necessary grating function ϕ_h for the holographic optical element, it is most convenient to find its grating vector first. This is best done by exploiting the propagation vectors of the input and output wavefronts. The normalized propagation vectors, which can be regarded as the direction cosines of the input ($\hat{\mathbf{K}}_i$) and output ($\hat{\mathbf{K}}_o$) rays, can be written as $\hat{\mathbf{K}}_i = (\lambda/2\pi)\nabla\phi_i$, $\hat{\mathbf{K}}_o = (\lambda/2\pi)\nabla\phi_o$, and the normalized grating vector $\hat{\mathbf{K}}_h = (\lambda/2\pi)\nabla\phi_h$, where ∇ is the gradient operator; ϕ_i and ϕ_o are the phases of the input and output wavefronts, respectively; and λ is the wavelength of light. The diffraction relation for the first diffraction order of the holographic element can now be written as $\hat{K}_{o_x} = \hat{K}_{i_x} + \hat{K}_{h_x}$, $\hat{K}_{o_y} = \hat{K}_{i_y} + \hat{K}_{h_y}$, $\hat{K}_{o_z} = (1 - \hat{K}_{o_x}^2 - \hat{K}_{o_y}^2)^{1/2}$. The element can thus be viewed as a combination of local gratings that change the direction of the incident rays of light according to the diffraction relation.

To obtain long focal depth, the holographic axilens would be composed of zones, each having a different focal length instead of a constant focal length f for the conventional lens. By choosing these zones to be concentric rings

with an infinitesimal width, the normalized grating vector of the hologram can be expressed in circular symmetry by a 1-D function as

$$\hat{K}_h(r) = \frac{-r}{[r^2 + f(r)^2]^{1/2}} \approx \frac{-r}{f(r)}, \tag{2}$$

assuming an incident input plane wave with $\hat{K}_{i_x} = \hat{K}_{i_y} = 0$, where r is the radial coordinate, $f(r)$ is a continuous function of the focal depth, and the preceding approximation exists for a low effective f-number. A general form for the variable focal length $f(r)$ can be the following monotonic function:

$$f(r) = f_o + ar^b, \tag{3}$$

where a, b, and f_o are constants. For a positive constant a, geometrical optics predicts that the focal range for an element with the focal length of Eq. (3) will be $f_o < z < f_o + aR^b$, where R is the radius of the element, so the extended focal depth $\Delta F = aR^b$.

The constant b depends on the desired intensity distribution of the central peak. For example, if it is required that the central peak throughout the focal range has uniform intensity, then the area of each ring having a focal distance between f and $f + \delta f$ should be the same. Since the area of such a ring is $r\delta r$, we can express this requirement as

$$\delta f(r) = 2ar\delta r. \tag{4}$$

Integrating Eq. (4) yields

$$f(r) = f_o + ar^2. \tag{5}$$

Equation (5) indicates that the requirement for uniform intensity distribution of the peak results in $b = 2$, so that $\Delta F = aR^2$, is the extended measuring range depth.

Finally, the phase function of the axilens can be calculated by integrating the grating vector of Eq. (2) and substituting the desired focal length given by Eq. (5). The grating function of the element is calculated by the relation $\phi_h(r) = (2\pi/\lambda)\int \hat{K}_h(r)dr$ yields

$$\phi_h(r) = -\frac{\pi}{\lambda a}\ln\{2a[a^2r^4 + (1 + 2f_oa)r^2 + f_o^2]^{1/2} + 2a^2r^2$$

$$+ 1 + 2f_oa\} \cong \frac{-\pi}{\lambda a}\ln\left(r^2 + \frac{f_o}{a}\right). \tag{6}$$

The approximation is valid for $af_o \gg 1$. Note that the analytic phase function of the axilens given by Eq. (6) can be improved by using it as an initial guess for an iterative design procedure, such as the Gerchberg-Saxton algorithm.[11]

The enlarging factor of the focal depth M_o is defined as the ratio between the extended focal depth of the holographic axilens and the monochromatic focal depth $\delta F = 6\lambda F_\#^2$ (50% of the maximal intensity), where $F_\#$ is the f-number of the element. With this definition we get

$$M_o = \frac{\Delta F}{\delta F}. \tag{7}$$

From a geometrical consideration, the resolvable depth of the system is given by

$$\delta z \cong \frac{\delta x_{\text{imag}}}{\sin \theta}, \tag{8}$$

where δx_{imag} is the resolvable lateral shift of the imaged light (the center) on the CCD. In general, the resolvable lateral shift of the light is proportional to the imaged spot itself, where the proportional constant depends on the accuracy required to determine the center of the image light distribution. A commonly used merit function to characterize the performance of the optical profilometer is the number of resolving depth steps (NRD):

$$\text{NRD} = \frac{\Delta F}{\delta z} = M_o \frac{\delta F}{\delta z}. \tag{9}$$

Equation (9) indicates that, for our device, the NRD can be increased by a factor of M_o, compared with the conventional single spot triangulation system, while maintaining the same lateral resolution.

3 Realization and Experimental Results

An automatic 3-D optical profilometer was designed, realized, and evaluated experimentally and theoretically for the acquisition and measurement of 3-D surfaces. For the illumination source a He-Ne laser was used at a wavelength of $\lambda = 633$ nm. The light emerging from the laser is expanded by using a 4-f system and is focused by the Axilens.

The parameters of the axilens was chosen $R = 12.5$ mm, $f_o = 1220$ mm, $\Delta F = 58$ mm, and the wavelength $\lambda = 633$ nm. For the experiment, the axilens was recorded as a computer-generated hologram using the Lee-type procedure.[9,12] Then a binary mask described by the grating function of Eq. (6) was realized using high-resolution laser lithography. The amplitude transmission for such a Lee-type binary mask can be derived as

$$t(x,y) = U_s[\cos(\phi_h) - \cos(\pi q)], \tag{10}$$

where U_s is the unit step function defined by

$$U_s(\eta) = \begin{cases} 1, & \eta \geq 0 \\ 0, & \eta < 0 \end{cases},$$

and where q is the duty cycle of the grating, which was chosen as 0.5. To separate the diffraction orders, a linear phase term of $2\pi \sin(\theta_x)/\lambda$ was added to the axilens phase function of Eq. (6). The off-axis angle θ_x was chosen as 0.05 rad, where x is one of the transverse coordinates.

To test the experimental arrangement of the profilometer, a series of measurements was performed on a flat object, placed at an angle so as to include the entire focal range in the measurements. First, the intensity cross section distributions of the reflected light were measured at several different locations along the focal range from the beginning
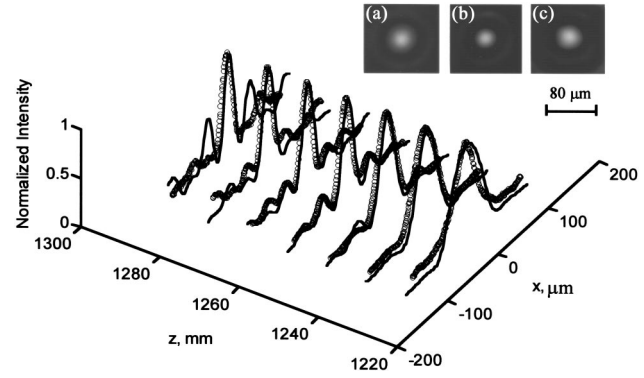

Fig. 2 Measured (circles) and calculated (solid curve) normalized intensity cross sections at several distances along the focal range for the holographic axilens. The inset shows the experimental imaged spots for three distances from the axilens: (a) $z = 1245$ mm, (b) $z = 1260$ mm, (c) $z = 1275$ mm.

of the focal range, $z = f_o = 1220$ mm, to the end of the focal range, $z = 1280$ mm. These measured intensity distributions were then compared with calculated values. For the simulation, the intensity distribution at any plane along the z axis was calculated by numerically solving the Fresnel diffraction integral:

$$I(z,r) = \left(\frac{2\pi}{\lambda z}\right)^2 \left| \int_0^R \exp\{i2\pi[r'^2/2\lambda z - \phi(r')]\} \right.$$
$$\left. \times J_0(2\pi r r'/\lambda z) r' \, dr' \right|^2, \tag{11}$$

where r denotes the radial position at the plane, and J_0 is the zero-order Bessel function. The experimental images of the spot size as well as the measured and the calculated cross sections are presented in Fig. 2. As is clearly evident, there is good agreement between the calculated and the measured intensity cross sections. Moreover, these results show that a diffraction-limited spot size of approximately $\Delta x \cong 40$ μm at FWHM is maintained throughout the focal range. Note that the sidelobes for the intensity distribution of the axilens are higher than for an Airy pattern that would be obtained with a spherical lens. The intensity distribution at any plane along the z axis was also measured and calculated. Figure 3 shows the normalized intensity distribution along the z axis $I(z, r=0)$ in the focal range of the axilens. For comparison, we present the corresponding distribution for a spherical holographic lens, which has the same aperture and focal distance of 1250 mm, $F_\# = 50$. As we can observe, the depth of focus is approximately six times greater for this axilens than for the spherical lens. Note that the absolute peak intensity is lower for the axilens. The intensity distribution of the conventional system is significantly broad beyond the focal depth $\delta F \cong 6\lambda F_\#^2 \cong 10$ mm, therefore the enlarging factor of the focal depth given by Eq. (7) is $M_o \cong 6$. The improvement of the axilens approach is clearly evident.

To determine the object resolvable depth of the system with the holographic Axilens, it is necessary to scan an object with a known surface topography and compare the
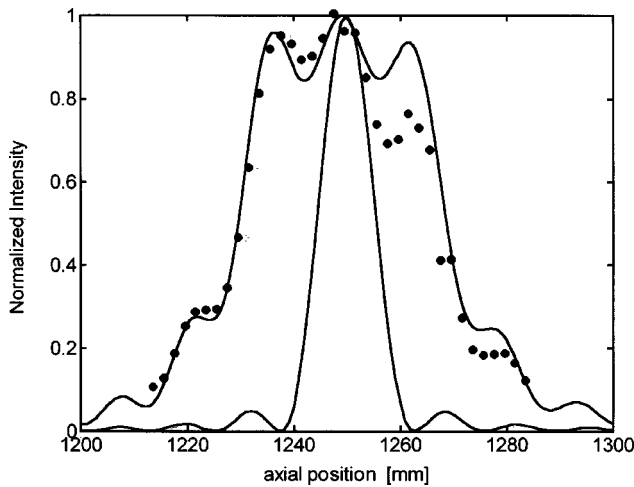
Fig. 3 Measured (dots) and calculated normalized intensity distribution as a function of the axial distance around the depth-measuring range for the axilens and the calculation for a spherical holographic lens.

Fig. 5 Three-dimensional surface topography of an rf aluminum antenna plate, which was obtained by optical profilometer based on holographic axilens.

measured results with the given surface. This was achieved with a flat object (a high-quality laser mirror) placed at an angle. The measured profile is shown in Fig. 4. For this measurement a 12-bit digital-cooled CCD camera, 1280 $\times$ 1224 pixels (Sensicam, PCO Computer Optics BMbH), and the centroid (center of gravity) algorithm were used to detect the center of the imaged spot.[13,14] The calculation of the centroid, which is the first moment of the imaged intensity distribution of the intersection point, is given by $\bar{x}_j = (\Sigma_i I_{ij} x_{ij})/(\Sigma_i I_{ij})$, where I_{ij} is the intensity value measured in pixel x_{ij}, and $\bar{x}_j$ is the coordinate of the centroid. The occurrence of error due to the discrete structure of the information can reach much below the CCD pixel size. The root mean square (rms) deviation of the measured results from the expected linear line was <0.6 μm. These results indicate that, for our lateral and depth resolutions of δx

$\cong \delta z \cong 0.6$ μm ($\theta = \pi/2$), and for the extended depth measuring range of $\Delta F \cong 58$ mm [according to Eq. (9)]; the NRD is seen to be $\cong 10^5$.

Finally, the profilometer used real-time software for reading the data from the CCD camera and processing the center calculations, so the time to complete a full 3-D scan of the object's surface was determined by the speed of the stepper motor. Figure 5 demonstrates, for example, the 3-D surface topography of an rf aluminum antenna plate, formed by a computer numerical control (CNC), which was obtained using the advanced method. The experimental results indicate that it is possible to measure a large depth of range without any decrease in the horizontal resolution by utilizing an axilens.

4 Conclusions

A method for a triangulation system based on the use of a holographic axilens with a large depth-measuring range without any decrease in the axial or the lateral resolution was described. The experiments yield 3-D surface measurements with lateral and depth optical resolutions of <0.6 μm, for a depth of focus of about 60 mm, resulting in 10^5 resolving depth steps.
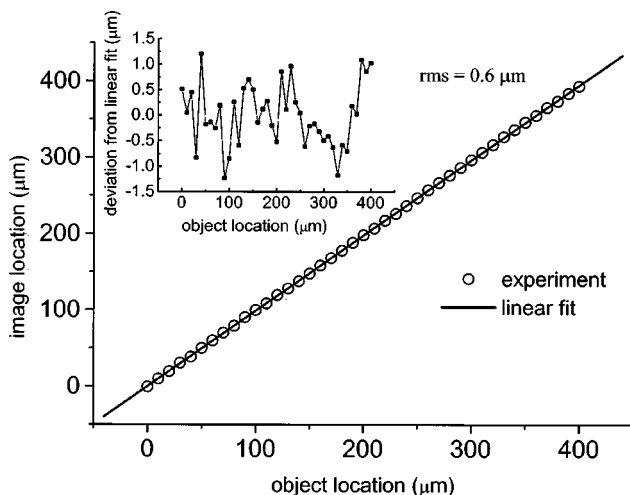

Fig. 4 Section of a measured profile of a flat object. Also shown is the expected object profile. The inset shows the deviation from a linear fit as a function of the object location.
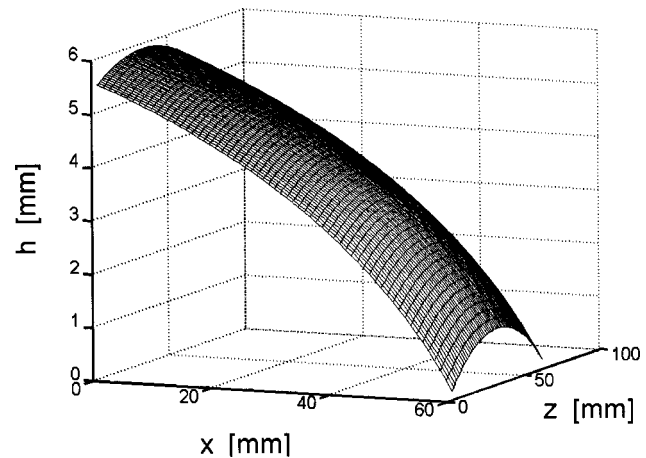
References

1. L. Jin, Y. Kodera, T. Yoshizawa, and Y. Otani, "Shadow moiré profilometry using the phase-shifting method," *Opt. Eng.* **39**, 2119–2123 (2000).
2. E. Hasman, N. Davidson, and A. A. Friesem, "Multifunctional holographic elements for surface measurements," *Opt. Eng.* **31**, 363–368 (1992).
3. M. Hartrumpf and R. Munser, "Optical three-dimensional measurements by radially symmetric structured light projection," *Appl. Opt.* **36**, 2923–2928 (1997).
4. R. G. Dorsch, G. Hausler, and J. M. Herrmann, "Laser triangulation: fundamental uncertainty in distance measurement," *Appl. Opt.* **33**, 1306–1314 (1994).
5. G. Bickel, G. Hausler, and M. Maul, "Triangulation with expanded range of depth," *Opt. Eng.* **24**, 975–977 (1985).
6. N. Davidson, A. A. Friesem, and E. Hasman, "Efficient formation of non-diffracting beams with uniform intensity along the propagation direction," *Opt. Commun.* **88**, 326–330 (1992).
7. N. Davidson, A. A. Friesem, and E. Hasman, "Holographic axilens: high resolution and long focal depth," *Opt. Lett.* **16**, 523–525 (1991).
8. E. Hasman and A. A. Friesem, "Analytic optimization for holographic optical elements," *J. Opt. Soc. Am. A* **6**, 62–72 (1989).
9. E. Hasman, N. Davidson, and A. A. Friesem, "Aspheric holographic

elements for far IR radiation,'' *Opt. Commun.* **89**, 306–315 (1992).
10. E. Hasman, N. Davidson, Y. Danziger, and A. A. Friesem, ''Diffractive optics: design, realization, and applications,'' *Fiber Integr. Opt.* **16**, 1–25 (1997).
11. R. W. Gerchberg and W. O. Saxton, ''A practical algorithm for the determination of phase for image and diffraction plane pictures,'' *Optik (Stuttgart)* **35**, 237–246 (1972).
12. W. H. Lee, ''Binary computer-generated holograms,'' *Appl. Opt.* **18**, 3661–3669 (1979).
13. J. Ares and J. Arines, ''Effective noise in thresholded intensity distribution: influence on centriod statistics,'' *Opt. Lett.* **26**, 1831–1833 (2001).
14. H. Canabal, J. Alonso, and E. Bernabeu, ''Laser beam deflectometry based on a subpixel resolution algorithm,'' *Opt. Eng.* **40**, 2517–2523 (2001).

Erez Hasman received his BSc degree in 1981 from the Tel Aviv University, his MSc degree in 1985 from the Technion, Haifa, and his PhD in 1992 from Weizmann Institute of Science, Rehovot, Israel. From 1981 to 1986 he was a senior scientist with the government of Israel, Department of Science, Haifa. From 1992 to 1994 he was chief physicist of the graphic and recognition products line with the Optrotech Company, performing research and development in the areas of photoploters and imaging systems for printed circuit boards and graphic arts industries. From 1994 to 1996 he was a technology analysis manager with the Elop Company in Israel, and a scientific consultant with the Weizmann Institute of Science. From 1996 to 1998 he was a senior visiting scientist with the Weizmann Institute of Science and a scientific consultant. He is currently an associate professor of optical sciences and heads the Optical Engineering Laboratory at the Technion-Israel Institute of Technology, Haifa, Faculty of Mechanical Engineering. He is concerned with subwavelength optical elements, diffractive optics, nano-optics, polarization state manipulations, optical metrology, optical storage, nonconventional laser resonators, and electro-optics devices. Prof. Erez Hasman is a member of OSA and SPIE.

Vladimir Kleiner received his MSc degree in 1971 from the Kharkov State University and his PhD degree in 1983 from the Institute of Low Temperature Physics, Ukraine Academy of Science, Kharkov. From 1971 to 1995 he was a research associate and headed the research group in the Institute for Physics and Technology, Academy of Sciences of Ukraine. From 1992 to 1994 he was an invited researcher with the Applied Physics Department, Chalmers University of Technology, Goteborg, Sweden. From 1997 to 1998 he was a researcher with the School of Physics and Astronomy at the Faculty of Exact Sciences, Tel-Aviv University, Israel. Since 1998 he has been a researcher with the Optical Engineering Laboratory at the Technion-Israel Institute for Technology, Faculty of Mechanical Engineering, Haifa. His research interests now include diffractive optics, subwavelength gratings, polarization state manipulations and geometric phases, nano-optics, and optical metrology. Dr. V. Kleiner is a member of OSA.